Journal of Power Sources 196 (2011) 3054–3059

Contents lists available at ScienceDirect

Journal of Power Sources

journal homepage: www.elsevier.com/locate/jpowsour

Characteristics of a fluidized bed electrode for a direct carbon fuel cell anode

Jubing Zhang[a], Zhaoping Zhong[a,*], Dekui Shen[a,b], Jianmin Xiao[a], Zongming Fu[a], Huiyan Zhang[a], Jinxiao Zhao[a], Weiling Li[a], Min Yang[a]

[a] School of Energy and Environment, Southeast University, Nanjing 210096, China
[b] School of Engineering Sciences, University of Southampton, Highfield, Southampton SO17 2BJ, UK

ARTICLE INFO

Article history:
Received 20 November 2010
Accepted 22 November 2010
Available online 26 November 2010

Keywords:
Fluidized bed electrode
Direct carbon fuel cell
Anode
Activated carbon
Limiting current density

ABSTRACT

The characteristics of a fluidized bed electrode applied as a direct carbon fuel cell anode, which has an inner diameter of 35 mm and height of 520 mm and employed bamboo-based activated carbon (BB-AC) as a feedstock, are vigorously studied under various experimental conditions. The optimal performance of the fluidized bed electrode direct carbon fuel cell (FEBDCFC) anode with the BB-AC as a fuel is obtained under the following conditions with a limiting current density of 95.9 mA cm^{-2}: reaction temperature, 923 K; N_2 flow rate, 385 ml min^{-1}; O_2/CO_2 flow rate, 10/20 ml min^{-1}; nickel particle content, 30 g; and a cylindrically curved nickel plate as a current collector. Under the same optimal conditions, the limiting current density of the FEBDCFC anode with oak wood-based activated carbon and activated carbon fiber as the fuel is determined to be 94.5 and 88.4 mA cm^{-2}, which is lower than that determined for BB-AC as the fuel. Comparatively, the limiting current density for graphite, which is utilized as the carbon fuel for this fuel cell system, could not be unequivocally determined because no plateau of the limiting current density against the overpotential is observed.

1. Introduction

The fuel cell is a well-established technology for converting the chemical energy of fuel into electrical energy through diverse electrochemical reactions [1–6]. The direct carbon fuel cell (DCFC) is considered to be a promising fuel cell device due to its outstanding characteristics for high energy conversion efficiency (nearly 100%) as estimated by the overall cell reaction (Eq. (1)), its lower emission when compared to that of coal-fired power plants and its flexibility in feedstock sources [7–10]. Moreover, the oxidation of carbon fuel could release more energy (20 kWh L^{-1}) when compared to other widely used fuels, such as hydrogen (2.4 kWh L^{-1}), methane (4.0 kWh L^{-1}), gasoline (9.0 kWh L^{-1}) and diesel (9.8 kWh L^{-1}) [7,11].

$$C + O_2 = CO_2 \quad (1)$$

Cherepy et al. [10] at Lawrence Livermore National Laboratory built a tilted orientation DCFC device with a paste of carbon particles (<10^{-4} m) in the melt as the anode; a maximum power density of 100 mW cm^{-2} at a current density and reaction temperature of 120 mA cm^{-2} and 1073 K, respectively, was obtained. Zecevic et al. [11] used a molten hydroxide electrolyte and a Fe-Ti alloy container as the cathode to investigate the performance of carbon rods from different sources; an average power output of 40 mW cm^{-2} at the maximum current density of 250 mA cm^{-2} was obtained. Tao [12] at CellTech Power constructed a DCFC with carbon black as the anode, $(ZrO_2)(HfO_2)_{0.02}(Y_2O_3)_{0.08}$ as the electrolyte and $La_{0.84}Sr_{0.16}MnO_3$ as the cathode, which yielded a power output of 50 mW cm^{-2} at 1275 K.

The fluidized bed electrode (FBE) is a three-dimensional electrode that was first developed in the 1960s [13–16]. The FBE demonstrates two significant advantages. First, the enhanced heat transfer due to increased gas flow reduces the temperature gradient significantly, which favors electrochemical reactions. Second, due to the high gas flow rate, the improved mass transfer [14] in the fluidized bed enhances the transfer of ionic species between fluidized particles and the environment, reducing the concentration polarization. Vatistas and Bartolozzi [17] introduced a three dimensional current feeder for the FBE to improve the current distribution in the fluidized bed and reduce the maldistribution of potential. Matsuno et al. [18,19] have applied the FBE into MCFC and AFC and investigated the polarization characteristics of the MCFC anode and AFC cathode under different experimental conditions. However, studies of the characteristics of DCFC equipped with a FBE [20] are limited in the literature.

A fluidized bed electrode direct carbon fuel cell (FBEDCFC) anode reactor was developed in this work to study its characteristics more fully. A set of experiments under different conditions, including

* Corresponding author. Tel.: +86 025 83794700; fax: +86 025 83794700.
E-mail address: zzhong@seu.edu.cn (Z. Zhong).

0378-7753/$ – see front matter © 2010 Elsevier B.V. All rights reserved.
doi:10.1016/j.jpowsour.2010.11.130

flow rates of N_2, O_2 and CO_2, reaction temperature, nickel particle content and the carbon fuel sources, were carried out to examine the polarization characteristics of the FBEDCFC anode.

2. Experimental

2.1. Materials

Bamboo-based activated carbon (BB-AC) was produced from bamboo scraps, which were activated by K_2CO_3 and impregnated by HNO_3 for surface modification and ash removal. Oak wood-based activated carbon (OWB-AC) was similarly prepared; however, nickel was loaded before HNO_3 impregnation to obtain a low electrical resistivity. The amount of carbon fuel used for each experiment was 10 g.

Potassium carbonate, lithium carbonate, activated carbon fiber (ACF), graphite and nickel particles were supplied by Sinopharm Chemical Reagent Co., Ltd., Xinjiang Westar Bioengineering Co., Ltd. (Shanghai Office), Sucheng Environment Equipment Ltd., Qindao Xinghe Graphite Co., Ltd. and Shenzhen Xinlilai Industrial Materials Co., Ltd., respectively. N_2, O_2 and CO_2 gases (99.99% purity for all) were obtained from Jiangsu Top Grand Petrifaction Industry Gas Co., Ltd.

2.2. FBEDCFC apparatus

Polarization characteristics of the activated carbon were examined on the self-designed FBEDCFC anode that is shown in Figs. 1 and 2. The anode was composed of a SUS-316L outer shell, an inner corundum tube, a gas distributor, a counter electrode, a current collector, a reference electrode, nickel particles and a gas preheater.

The inner corundum tube was 520 mm in height with an external diameter of 45 mm and an inner diameter of 35 mm. The SUS-316L 840 mesh powder-sintered plate had a 45 mm diameter and was 8 mm thick; this plate was used as a gas distributor. The reference electrode was a closed-end corundum tube (8 mm external diameter, 550 mm length) with a gold wire (0.6 mm diameter) inside. A 1-mm diameter hole at the bottom of the corundum tube was present to facilitate the carbonate ion transfer. The corundum tube was sheathed by the other closed-end corundum tube (12 mm external diameter, 10 mm inner diameter, 60 mm length) to minimize contamination of the reference electrode melted by anode gas. The two closed-end corundum tubes in the reference electrode were connected with high temperature inorganic adhesive. The reference electrode was in equilibrium with the gas mixture (33% O_2 and 67% CO_2 according to cathode reaction shown in Eq. (2)), which was fed through the inner corundum tube at different gas flow rates (Fig. 3).

$$O_2 + 2CO_2 + 4e^- = 2CO_3^{2-} \quad (2)$$

Fig. 4 shows the two different types of current collectors: one was a flat nickel plate (50 mm × 32 mm × 0.4 mm) and the other was a cylindrically curved nickel plate (50 mm × 120 mm × 0.4 mm). The counter electrode was of the same dimensions as the cylindrically curved nickel plate current collector. Both the current collector and the counter electrode were connected to alumina-sheathed nickel wires 2 mm in diameter.

2.3. Testing procedure for the determination of polarization characteristics

Prior to the experiment, the current collector and counter electrode were polished with sandpaper and sequentially rinsed with distilled water and acetone [18]. The electrolyte was a mixture of 62 mol% Li_2CO_3 and 38 mol% K_2CO_3 with a total weight of 350 g. Two electric furnaces were used to heat the half cell, and each

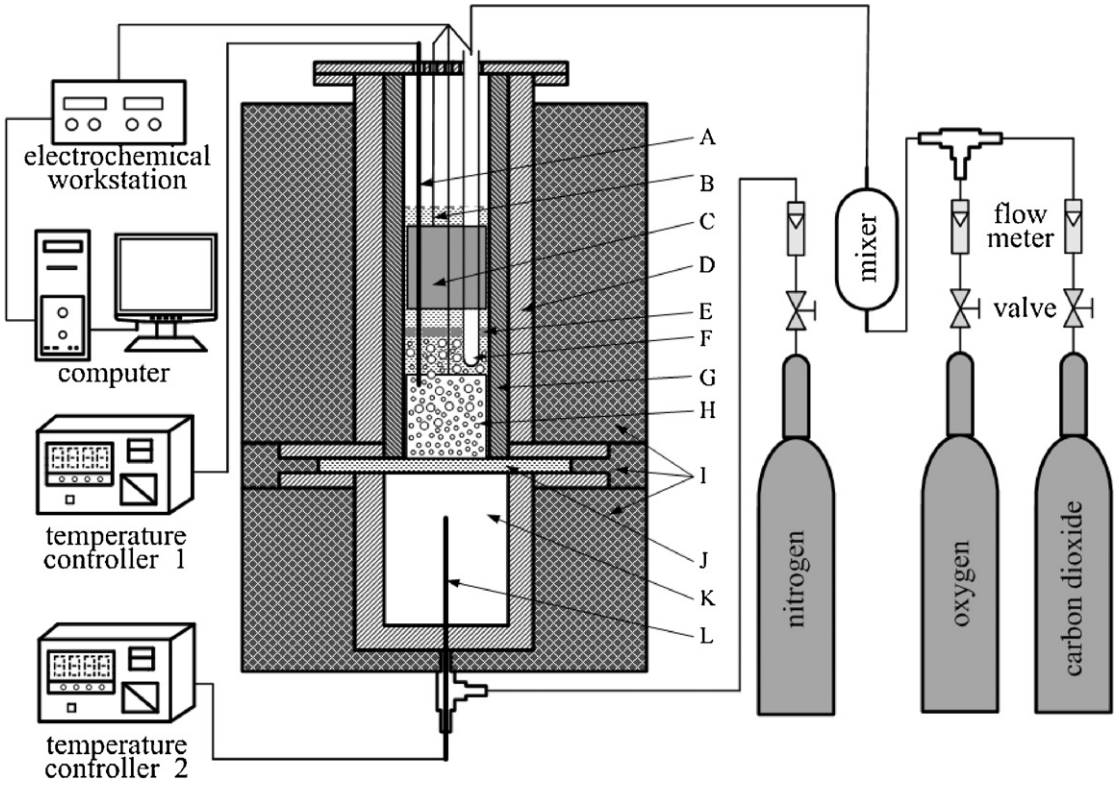

Fig. 1. Diagram of the FBEDCFC system for the polarization performance test. A: thermocouple 1; B: molten carbonate; C: counter electrode; D: 316L stainless steel tube; E: perforated plate; F: reference electrode; G: corundum pipe; H: current collector; I: electric furnace; J: gas distributor; K: air preheater; and L: thermocouple 2.

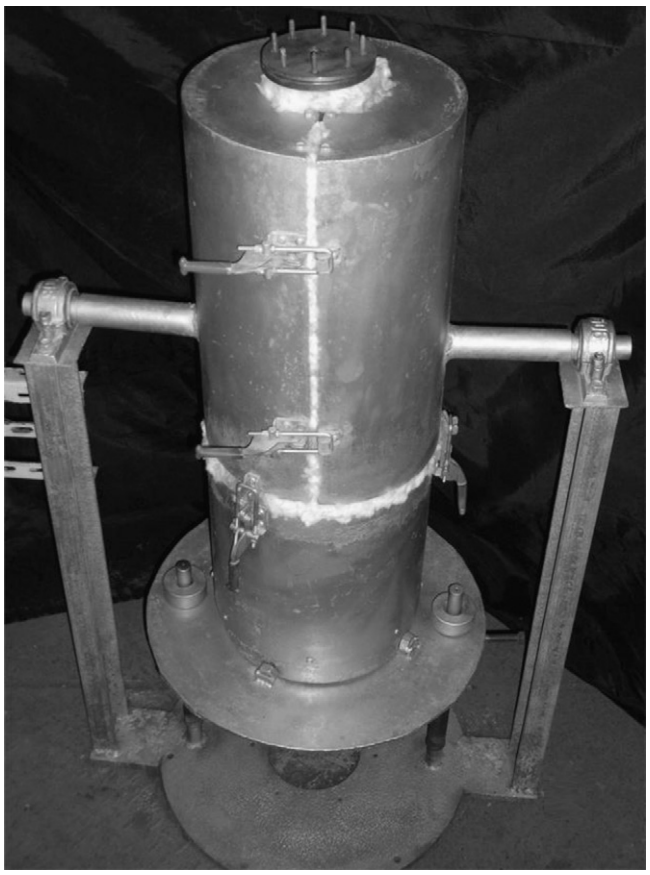

Fig. 2. The photo of the FBEDCFC anode.

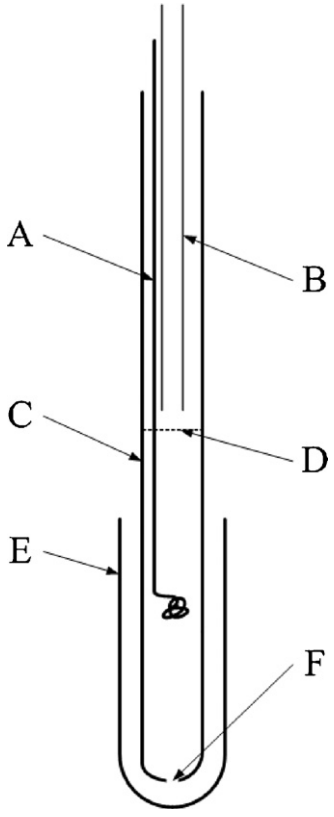

Fig. 3. Diagram of the reference electrode. A: gold wire; B: inlet tube; C: closed-end alumina tube; D: melt lever; E: closed-end alumina tube; and F: 1 mm hole.

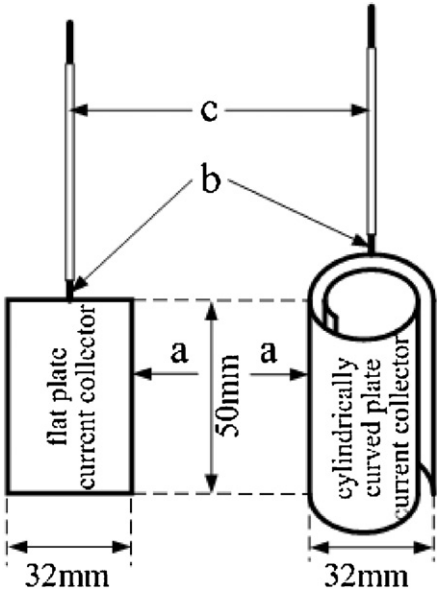

Fig. 4. Diagram of the current collector. a: nickel plate; b: nickel wire; and c: alumina tube.

of the furnaces was maintained at a constant temperature by an independent temperature controller. Both of the temperatures were measured using thermocouples, and the thermocouple connected to the upper electric furnace was protected by an alumina sheath against the caustic electrolyte. The fluidizing gas (N_2) was pre-heated before being fed into the anode through the gas distributor.

The current collector and the mixture of activated carbon and nickel particles were placed at the bottom of the anode. The perforated plate was fixed in the expected position for the activated carbon contacting with nickel particles rather than suspending on the surface of the molten carbonate. The counter electrode, reference electrode and carbonate were placed in anode in turn. The cover was then closed, and the half cell was heated to the fixed temperature. Finally, the circuit connection was completed to start the anode polarization performance test under different conditions. The steady-state polarization curves for the anode were measured using a CS150 electrochemical workstation provided by Wuhan Corrtest Instrument Co., Ltd.

To prevent the oxidation of the nickel particles, the current collector and counter electrode, N_2 gas was flushed through the whole system during the heating process. This process also prevented the leakage of carbonate from the gas distributor to the gas preheater.

3. Results and discussion

Polarization curves for the FBEDCFC anode for different carbon fuels (BB-AC, OWB-AC, ACF and graphite) obtained with the electrochemical workstation were established to evaluate the anode performance under different experimental conditions, as shown in Table 1.

3.1. Effect of N_2 flow rate

Polarization curves for the anode under different N_2 flow rates are shown in Fig. 5. As the N_2 flow rate is increased from 75 to 275 ml min^{-1}, the limiting current density of the anode increases from 80.1 to 97.5 mA cm^{-2}. The increase in the N_2 flow rate strengthens the turbulence in the anode, enhancing the transfer of the reactant from the environment to the working electrode

Table 1
Experimental conditions.

No.	Gas flow rate (ml min^{-1})		Temperature (K)	Nickel particle content (g)	Current collector	Fuel type
	N_2	O_2/CO_2				
1	75	10/20	650	30	[a]	BB-AC
2	140	10/20	650	30	[a]	BB-AC
3	275	10/20	650	30	[a]	BB-AC
4	385	10/20	650	30	[a]	BB-AC
5	385	5/10	650	30	[a]	BB-AC
6	385	15/30	650	30	[a]	BB-AC
7	385	10/20	600	30	[a]	BB-AC
8	385	10/20	625	30	[a]	BB-AC
9	385	10/20	675	30	[a]	BB-AC
10	385	10/20	650	0	[a]	BB-AC
11	385	10/20	650	15	[a]	BB-AC
12	385	10/20	650	45	[a]	BB-AC
13	385	10/20	650	30	[b]	BB-AC
14	385	10/20	650	30	[a]	OWB-AC
15	385	10/20	650	30	[a]	ACF
16	385	10/20	650	30	[a]	Graphite

[a] Cylindrically curved plate current collector.
[b] Flat plate current collector.

surface and the transfer of product from the working electrode surface to the environment. This enhanced process results in the decrease of the concentration polarization. Additionally, collision among the particles and the current collector are strengthened, accelerating the electrochemical reactions and improving current collection efficiency. As a result, both the current density and the limiting current density are enhanced with the increase in N_2 flow rate. However, the polarization curve reaches a steady state when the N_2 flow rate exceeds 275 ml min^{-1}.

3.2. Effect of O_2/CO_2 flow rate

The influence of the O_2/CO_2 flow rate on the polarization curve is shown in Fig. 6. When the O_2 flow rate is varied from 5 to 15 ml min^{-1}, the limiting current density of the anode reaches from 87.7 to 96.1 mA cm^{-2}. The increase in the O_2/CO_2 flow rate increases the reactant concentration in the molten carbonate, accelerating the electrochemical reactions. The mass transfer in the reference electrode is also enhanced by the increase in the O_2/CO_2 flow rate, resulting in the reduction of the concentration polarization. However, the polarization curve reaches a steady state when the O_2/CO_2 flow rate reaches 10/20 ml min^{-1}. This result might be attributed to the limited solubility of O_2 and CO_2 in the molten carbonate.

3.3. Effect of reaction temperature

Fig. 7 shows the influence of reaction temperature on the anode polarization curve. Both the current density and the limiting current density are enhanced as the reaction temperature is elevated. High temperature could improve the reactivity of the activated carbon and accelerate the anode reactions, releasing more free electrons. Moreover, the conductivity of the molten carbonate is also enhanced by the temperature, which may reduce the ohmic polarization in the anode. However, the use of ultra high temperature is not applicable in this cell because the corrosion of stainless steel and loss of electrolyte would inevitably occur.

3.4. Effect of nickel particle content

Fig. 8 shows the polarization curves for the anode with different nickel particle contents. The limiting current density for the anode with a nickel particle content of 30 g is nearly 1.5 times that of the limiting current density observed for the anode without nickel

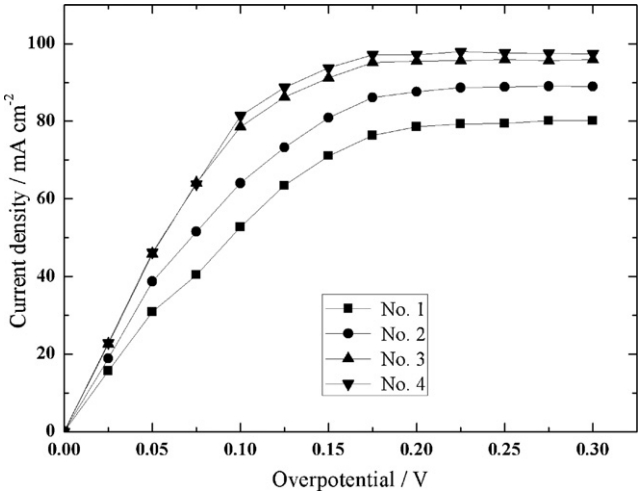

Fig. 5. Polarization curves for the anode at different N_2 flow rates.

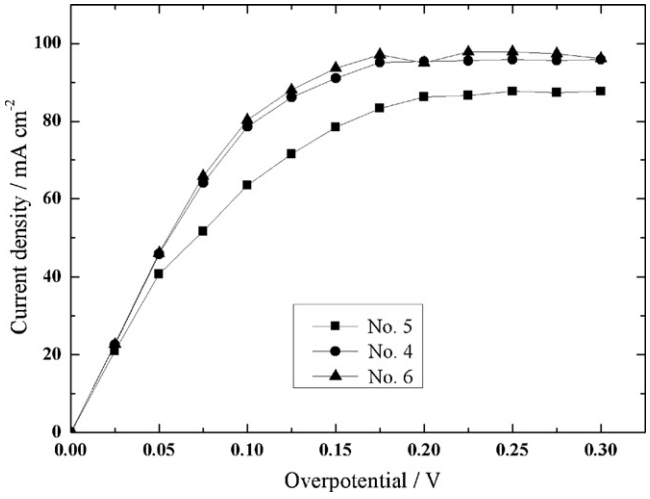

Fig. 6. Polarization curves for the anode at different O_2/CO_2 flow rates.

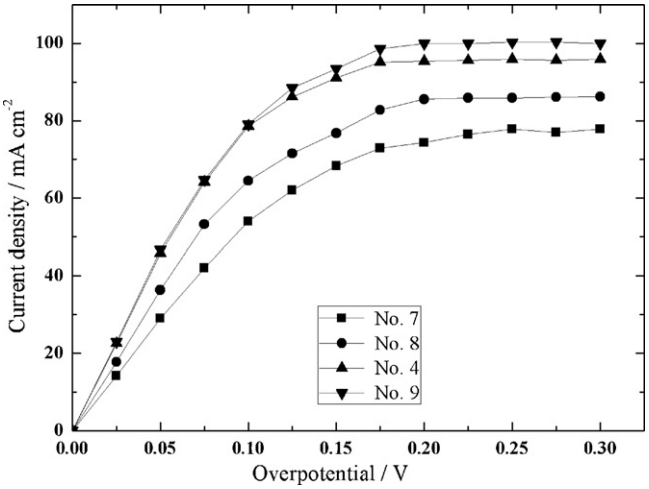

Fig. 7. Polarization curves for the anode at different reaction temperatures.

particles. The increase in the nickel particle content improves the contact area between the carbon fuel and the catalyst, promoting the electrochemical reactions in the anode. More free electrons would then be released, resulting in the larger current density. Notably, the polarization curve is only slightly changed when nickel particle content in the anode is over 30 g.

3.5. Effect of current collector type

Fig. 9 shows the polarization curves for the anode with different current collectors. The polarization curve of the anode with the cylindrically curved nickel plate current collector yields a higher limiting current density (95.9 mA cm^{-2}) compared to that of the anode with the flat nickel plate current collector (75.9 mA cm^{-2}). A cylindrically curved nickel plate current collector enlarges the surface area of the catalyst, which favors the contact probability between the nickel particles and the current collector and promotes the efficiency of current collection. Thus, a better performance of the FBEDCFC anode with a cylindrically curved nickel plate current collector than that with a flat nickel plate current collector is observed.

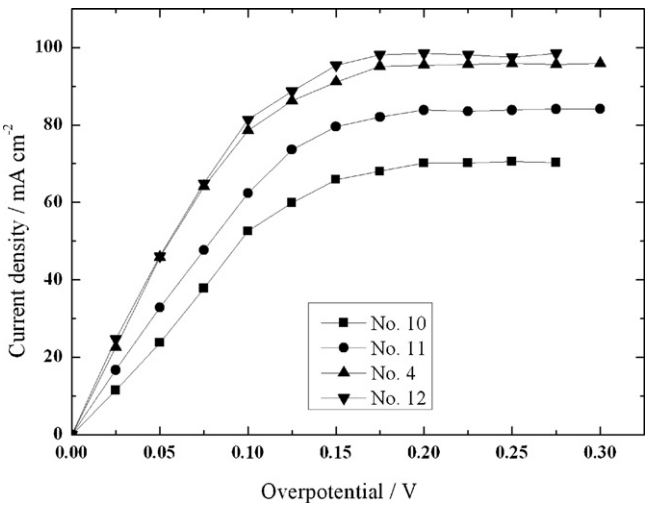

Fig. 8. Polarization curves for the anode with different nickel particle contents.

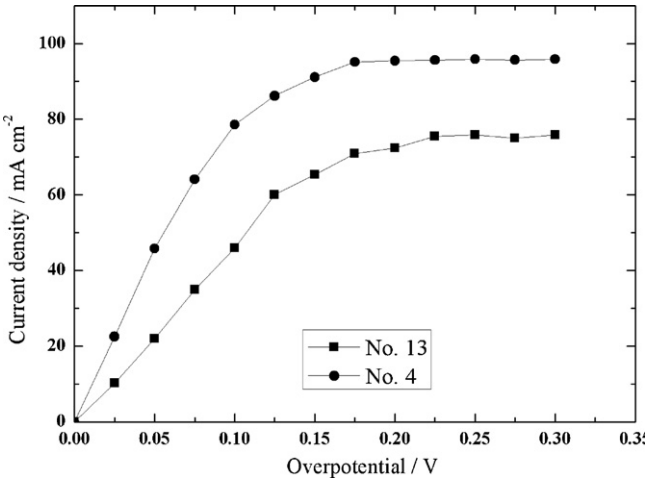

Fig. 9. Polarization curves for the anode with different current collector types.

Table 2
Characteristics of different carbon fuels.

Fuel type	BB-AC	OWB-AC	ACF	Graphite
BET surface area (m^2 g^{-1})	1281	1197	1573	35
Electrical resistivity (μΩ m)	1679.5	2047.2	2214.7	42.3
Ash content (%)	1.97	3.65	2.41	0.23

3.6. Effect of carbon fuel sources

The polarization curves of the anode with different carbon fuels are shown in Fig. 10. The testing conditions were as follows: reaction temperature, 923 K; N_2 flow rate, 385 ml min^{-1}; O_2/CO_2 flow rate, 10/20 ml min^{-1}; nickel particle content, 30 g; and a cylindrically curved nickel plate current collector. The characteristics of the four carbon fuels are displayed in Table 2 in terms of BET surface area, electrical resistivity and ash content. The FTIR spectra for the carbon fuels are shown in Fig. 11.

The limiting current density of the anode with BB-AC, OWB-AC and ACF is estimated to be 95.9, 94.5 and 88.4 mA cm^{-2}, respectively, but no limiting current density for graphite could be observed due to the ambiguous plateau of the current density against the overpotential (Fig. 10). According to the current density found from each polarization curve, the performance of the

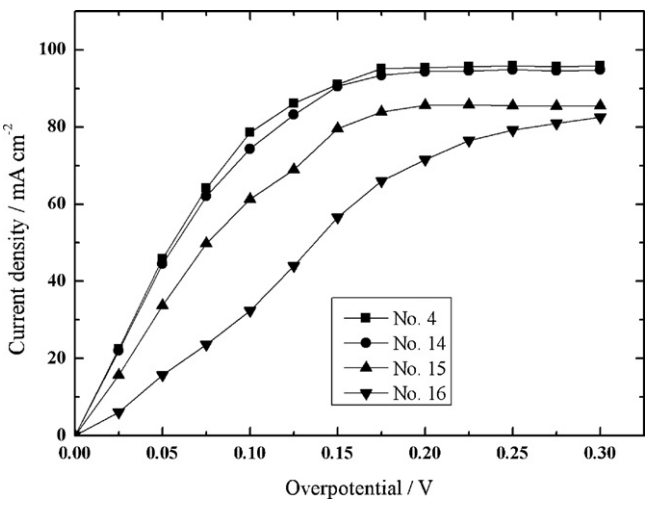

Fig. 10. Polarization curves for the anode with different carbon fuels.

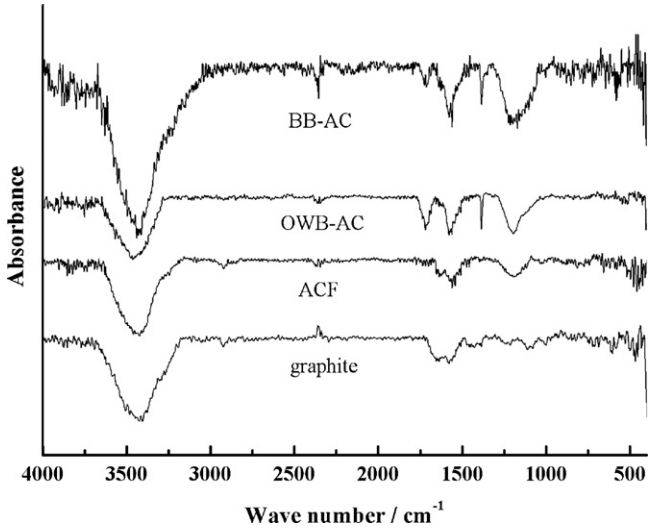

Fig. 11. FTIR spectra for different carbon fuels.

carbon fuels in the FBEDCFC anode may be ranked as BB-AC > OWB-AC > ACF > graphite.

The electrochemical polarization is restrained by the high BET surface area and high content of oxygen functional groups, and the ohmic polarization is enhanced by the high electrical resistivity. The BET surface area of ACF ($1573\,m^2\,g^{-1}$) is larger than that of self-made activated carbons (BB-AC ($1281\,m^2\,g^{-1}$), OWB-AC ($1197\,m^2\,g^{-1}$)). However, the content of surface oxygen functional groups in ACF is lower than that in self-made activated carbons. Moreover, ACF has a higher electrical resistivity ($2214.7\,\mu\Omega\,m$) than the two self-made activated carbons. Thus, the self-made activated carbons perform better than ACF in the FBEDCFC anode due to the balanced effects of the intrinsic properties of the carbon fuels, such as surface oxygen functional groups, BET surface area and electrical resistivity. Comparatively, the performance of BB-AC in the FBEDCFC anode is better than that of OWB-AC, probably due to the higher BET surface area, lower electrical resistivity and higher content of surface oxygen functional groups. Considering that graphite exhibits the best electrical conductivity (lowest electrical resistivity, $42.3\,\mu\Omega\,m$), its poor performance among the three carbon fuels in the FBEDCFC anode may be attributed to having the lowest BET surface area and a relatively low content of surface oxygen functional groups.

4. Conclusions

The polarization performance of the FBEDCFC anode under different experimental conditions was extensively investigated, and optimal conditions were obtained for BB-AC using a cylindrically curved nickel plate current collector with an N_2 flow rate of $385\,ml\,min^{-1}$, an O_2/CO_2 flow rate of $10/20\,ml\,min^{-1}$, a reaction temperature of 923 K and a nickel particle content of 30 g. Among the four different carbon fuels tested in the FBEDCFC anode, the BB-AC gave an outstanding polarization performance over the other three carbon fuels (OWB-AC, ACF and graphite) due to the balanced effects of the relevant properties, including the BET surface area, electrical resistivity and surface oxygen functional groups.

Acknowledgments

The support of the National Natural Science Fund Program of China (50776019), the Doctorial Subject Science & Technology Fund Program of the State Education Ministry of China (200802860038) and the Science & Technology Foundation of Southeast University of China (XJ0703267) are gratefully acknowledged.

References

[1] E. Gulzow, Alkaline fuel cells: a critical view, J. Power Sources 61 (1996) 99–104.
[2] K. Kordesch, V. Hacker, J. Gsellmann, M. Cifrain, G. Faleschini, P. Enzinger, R. Fankhauser, M. Ortner, M. Muhr, R.R. Aronson, Alkaline fuel cells applications, J. Power Sources 86 (2000) 162–165.
[3] S. Gamburzev, A.J. Appleby, Recent progress in performance improvement of the proton exchange membrane fuel cell (PEMFC), J. Power Sources 107 (2002) 5–12.
[4] N. Sammes, R. Bove, K. Stahl, Phosphoric acid fuel cells: fundamentals and applications, Curr. Opin. Solid State Mater. Sci. 8 (2004) 372–378.
[5] K. Joon, Critical issues and future prospects for molten carbonate fuel cells, J. Power Sources 61 (1996) 129–133.
[6] M.C. Williams, J.P. Strakey, W.A. Surdoval, L.C. Wilson, Solid oxide fuel cell technology development in the U.S., Solid State Ionics 177 (2006) 2039–2044.
[7] D.X. Cao, Y. Sun, G.L. Wang, Direct carbon fuel cell: fundamentals and recent developments, J. Power Sources 167 (2007) 250–257.
[8] G.A. Hackett, J.W. Zondlo, R. Svensson, Evaluation of carbon materials for use in a direct carbon fuel cell, J. Power Sources 168 (2007) 111–118.
[9] X. Li, Z.H. Zhu, J.L. Chen, R. De Marco, A. Dicks, J. Bradley, G.Q. Lu, Surface modification of carbon fuels for direct carbon fuel cells, J. Power Sources 186 (2009) 1–9.
[10] N.J. Cherepy, R. Krueger, K.J. Fiet, A.F. Jankowski, J.F. Cooper, Direct conversion of carbon fuels in a molten carbonate fuel cell, J. Electrochem. Soc. 152 (2005) A80–A87.
[11] S. Zecevic, E.M. Patton, P. Parharni, Carbon–air fuel cell without a reforming process, Carbon 42 (2004) 1983–1993.
[12] T. Tao, US Patent No. 6,692,861 (2004).
[13] N. Bharucha, P. Claessens, US Patent No. 3,941,669 (1976).
[14] J. Hiddleston, A. Douglas, Fluidized bed electrodes-fundamental measurements and implications, Nature 218 (1968) 601–602.
[15] B.K. Ferreira, Three-dimensional electrodes for the removal of metals from dilute solutions: a review, Miner. Process. Extr. Metall. Rev. 29 (2008) 330–371.
[16] M. Fleischmann, J. Oldfield, L. Tennakoon, Fluidized bed electrodes: part IV. Electrodeposition of copper in a fluidized bed of copper-coated spheres, J. Appl. Electrochem. 1 (1971) 103–112.
[17] N. Vatistas, M. Bartolozzi, A three-dimensional current feeder for fluidized bed electrodes, J. Appl. Electrochem. 20 (1990) 951–954.
[18] Y. Matsuno, A. Tsutsumi, K. Yoshida, Characteristics of three-dimensional electrodes for a molten carbonate fuel cell anode, Int. J. Hydrogen Energy 20 (1995) 601–605.
[19] Y. Matsuno, K. Suzawa, A. Tsutsumi, K. Yoshida, Characteristics of three-phase fluidized-bed electrodes for an alkaline fuel cell cathode, Int. J. Hydrogen Energy 21 (1996) 195–199.
[20] S. Li, A.C. Lee, R.E. Mitchell, T.M. Gur, Direct carbon conversion in a helium fluidized bed fuel cell, Solid State Ionics 179 (2008) 1549–1552.